Mon. Not. R. Astron. Soc. **399,** 121–128 (2009) doi:10.1111/j.1365-2966.2009.15291.x

Confirming a population of hot-dust dominated, star-forming, ultraluminous galaxies at high redshift

C. M. Casey,[1⋆] S. C. Chapman,[1] R. J. Beswick,[2] A. D. Biggs,[3] A. W. Blain,[4] L. J. Hainline,[5] R. J. Ivison,[6,7] T. W. B. Muxlow[2] and Ian Smail[8]

[1]*Institute of Astronomy, University of Cambridge, Madingley Road, Cambridge, CB3 0HA*
[2]*Jodrell Bank Centre for Astrophysics, University of Manchester, Oxford Road, Manchester M13 9PL*
[3]*European Southern Observatory, Garching D-85748, Germany*
[4]*Department of Astronomy, California Institute of Technology, 1200 E California Blvd, Pasadena, CA 91125, USA*
[5]*Department of Astronomy, University of Maryland, College Park, MD 20742, USA*
[6]*UK Astronomy Technology Centre, Royal Observatory, Blackford Hill, Edinburgh EH9 3HJ*
[7]*Institute for Astronomy, University of Edinburgh, Blackford Hill, Edinburgh EH9 3HJ*
[8]*Institute for Computational Cosmology, Durham University, South Road, Durham DH1 3LE*

Accepted 2009 June 19. Received 2009 June 19; in original form 2008 May 26

ABSTRACT

We identify eight $z > 1$ radio sources undetected at 850 μm but robustly detected at 70 μm, confirming that they represent ultraluminous infrared galaxies (ULIRGs) with hotter dust temperatures ($\langle T_{\rm d} \rangle = 52 \pm 10$ K) than submillimetre galaxies (SMGs) at similar luminosities and redshifts. These galaxies share many properties with SMGs: ultraviolet spectra consistent with starbursts, high stellar masses and radio luminosities. We can attribute their radio emission to star formation since high-resolution Multi-Element Radio Linked Interferometer Network (MERLIN) radio maps show extended emission regions (with characteristic radii of 2–3 kpc), which are unlikely to be generated by active galactic nucleus (AGN) activity. These observations provide the first direct confirmation of hot, dusty ULIRGs which are missed by current submillimetre surveys. They have significant implications for future observations from the *Herschel Space Observatory* and Submillimetre Common-User Bolometer Array 2 (SCUBA2), which will select high-redshift luminous galaxies with less selection biases.

Key words: galaxies: evolution – galaxies: formation – galaxies: high-redshift – galaxies: starburst – cosmology: observations.

1 INTRODUCTION

The most luminous starbursts in the Universe signal a rapid growth phase in galaxies. Submillimetre galaxies (SMGs) (bright infrared luminous galaxies with $S_{850} \gtrsim 2$ mJy at $\langle z \rangle = 2.2$; e.g. Blain et al. 2002; Smail et al. 2002; Chapman et al. 2005) represent some of the best studied ultraluminous starbursts at high-z, and they are likely building some of the most massive galaxies found at the present epoch. However, it has been suggested that selecting $z = 1$–3 galaxies by their submillimeter emission is prone to finding specimens with cold average dust temperatures (e.g. Eales et al. 2000; Blain et al. 2004; Chapman et al. 2004) leaving the possibility of a large population of hotter ultraluminous infrared galaxies (ULIRGs) at high redshift.

The far-infrared (FIR) part of the spectrum (8–1000 μm) is dominated by the reprocessed emission from dust and resembles a modified blackbody whose most important variable is the characteristic dust temperature, $T_{\rm d}$ (Blain et al. 2002). At $z \sim 2$, the mean redshift of SMGs, submillimetre observations at 850 μm sample the emission at a strongly sloped section of the blackbody, the Rayleigh–Jeans tail, where the flux is approximated as $S_{850} \approx T_{\rm d}^{-3.5}$ for a given $L_{\rm FIR}$. For example, if $T_{\rm d}$ rises (for fixed $L_{\rm FIR}$), the peak flux shifts towards shorter wavelengths, away from observed 850 μm and the submillimeter (submm) flux can easily drop beneath the submm confusion limit (∼2 mJy for JCMT; Blain 1999). Current submm instruments restrict studies to those ULIRGs with cooler dust temperatures ($T_{\rm d} < 40$ K) or the highest luminosities ($L > 10^{13}$ L$_\odot$), potentially missing a substantial portion of the luminous starbursts at high redshift.

Observations of local ULIRGs (e.g. *IRAS* 60 μm starbursts; Levine et al. 1998) suggest that dust temperatures can vary substantially in star-forming systems, from 20 up to 100 K. For a 10^{13} L$_\odot$ local ULIRG, the mean dust temperature is 45 K (Rieke et al. 2009) higher than 36 K, the mean temperature of similar luminosity SMGs at $z \sim 1$–3. A handful of individual ULIRGs at high redshift have been found to have characteristic dust temperatures around 50–80 K (e.g. FSC 10214+4724, Cloverleaf Quasar, IRAS F15307+3252,

⋆E-mail: ccasey@ast.cam.ac.uk

Table 1. Observed and derived properties of hot-dust ULIRGs.

Name	z	$S_{1.4\,\mathrm{GHz}}$ (μJy)	S_{70} (mJy)	S_{850} (mJy)	S_{1200} (mJy)	S_{24} (μJy)	$L_{\mathrm{X[2-10\,keV]}}$ (erg s^{-1})	L_{FIR} (L$_\odot$)	SFR (M$_\odot$ yr^{-1})	$M_\star$ (M$_\odot$)	R_{eff} (kpc)	T_{d} (K)
RG J123710.60+622234.6	1.522	38.3 ± 10.1	3.9 ± 0.5	<1.8	<1.8	227 ± 39	$<9.6 \times 10^{42}$	1.4×10^{12}	247^{+75}_{-57}	1.2×10^{11}	1.7	54 ± 3
RG J123653.37+621139.6	1.275	86.7 ± 8.3	6.6 ± 0.4	<1.4	<0.7	164 ± 33	2.2×10^{42}	2.0×10^{12}	349^{+35}_{-32}	1.7×10^{11}	2.9	47 ± 1
RG J123645.89+620754.1	1.433	83.4 ± 9.8	4.8 ± 0.4	<6.3	<1.6	172 ± 34	5.1×10^{42}	2.7×10^{12}	458^{+57}_{-52}	3.0×10^{11}	2.1	48 ± 1
RG J105159.90+571802.4	1.047	74.5 ± 5.6	7.7 ± 1.2	<5.9	<1.4	738 ± 27	$<2.2 \times 10^{42}$	1.0×10^{12}	179^{+14}_{-13}	6.6×10^{10}	2.7	46 ± 2
RG J105154.19+572414.6	0.922	45.4 ± 6.3	6.1 ± 0.9	<4.3	<1.7	510 ± 22	$<1.6 \times 10^{42}$	4.6×10^{11}	79^{+12}_{-10}	8.3×10^{10}	2.0	45 ± 3
RG J105146.61+572033.4	2.383	33.5 ± 5.8	9.5 ± 1.1	<2.4	<3.1	298 ± 16	$<1.4 \times 10^{43}$	4.1×10^{12}	709^{+120}_{-120}	2.7×10^{11}	2.1	72 ± 3
ULIRGs with AGN:												
RG J123711.34+621331.0	1.996	126.3 ± 8.6	1.4 ± 0.4	<6.0	<4.4	473 ± 57	1.9×10^{43}	9.7×10^{12}	-	3.5×10^{11}	3.7	50 ± 2
RG J123711 SF component:		79.6 ± 17.2						6.1×10^{12}	1047^{+120}_{-107}			
RG J123649.66+620738.0	2.315	327.0 ± 8.6	5.8 ± 0.4	<8.4	<1.1	912 ± 78	1.3×10^{45}	3.7×10^{13}	-	8.1×10^{10}	2.7	57 ± 1
RG J123649 SF component:		196.6 ± 17.2						2.2×10^{13}	3843^{+171}_{-164}			

Note. Observed and derived properties of the eight submm-faint radio galaxies detected at 70 μm. SFR and L_{FIR} are derived from radio luminosities, $\mathrm{M}_\star$ from stellar population model fits and T_{d} from modified blackbody FIR continuum fits constrained by 70 μm flux densities and normalized to radio luminosity. The temperature uncertainties stated here do not take the uncertainty in the FIR/radio correlation into account (as described in section 3.1). All sources are undetected at 850 and 1200 μm; the fluxes in the corresponding columns are 2σ upper limits. Two sources have AGN in addition to luminous star formation (RG J123711 and RG J123649); their L_{FIR} and SFR have been adjusted to represent just the star-forming components in the abbreviated rows 'RG J ... SF component:'; the star-forming components have been carefully deconvolved from AGN emission in the MERLIN maps as discussed in Section 3.4. The effective radius, R_{eff}, is the circularized radius corresponding to a surface area of the $>3\sigma$ MERLIN radio emitting region.

APM08297+5255). However, they are either exceptionally luminous or strongly lensed, thus detectable at 70, 850 and 1200 μm wavelengths with the sensitivity of current instruments. This hints that submm selection may indeed be biased towards colder dust specimens, missing some fraction of hotter dust ULIRGs at high redshift.

At $z \sim 1$–3, many galaxies with hot dust could exist but are difficult to detect and study as a population. The first observational effort to characterize these 'hotter ULIRGs' came in Chapman et al. (2004), with a selection of submm-faint radio-selected galaxies with starburst optical/near-IR spectra, similar to SMGs. Since they had similar radio luminosities, redshifts and optical spectra to SMGs, they were thought to be ULIRGs. However, poor constraints on their FIR luminosities provided insufficient evidence of their high bolometric luminosity.

We present eight examples of ULIRGs where observations suggest hot dominant dust temperatures. Section 2 describes the data and our observations, Section 3 discusses the galaxies' physical properties and Section 4 discusses the selection biases prominent at FIR wavelengths and the context of hot-dust ULIRGs in other $z \sim 2$ galaxy populations. Throughout, we use AB magnitudes and assume $H_0 = 71\,\mathrm{km\,s^{-1}\,Mpc^{-1}}$ and $\Omega_0 = 0.27$ (Hinshaw et al. 2009).

2 SAMPLE AND OBSERVATIONS

We identified 44 potential hot high-z ULIRGs using the Chapman et al. (2004) optically faint radio galaxy (OFRG, also submm-faint, star-forming radio galaxy, SFRG) selection in the GOODS-N and Lockman Hole fields. They were detected in the ultradeep Very Large Array (VLA) radio maps of Biggs & Ivison (2006) ($S_{1.4\,\mathrm{GHz}} > 15$ μJy, $>3\sigma$). Spectroscopic follow-up of these potential ULIRGs with Keck Low Resolution Imaging Spectrometer (LRIS) revealed starburst spectral features (Chapman et al. 2004; Reddy et al. 2006), mostly at redshifts $z \gtrsim 1$. Obvious spectral active galactic nuclei (AGN) were not included in the sample. There were 26 Great Observatories Origins Deep–North (GOODS-N) sources and 18 Lockman Hole galaxies selected by this radio/rest-UV spectra method. Their redshift distribution (quartile of $z = 1.2$–2.6) is similar to the redshift distribution of radio-selected SMGs (quartile of $z = 1.2$–2.8).

The *Spitzer* 70 μm maps of GOODS-N and Lockman Hole are used for further selection. From the sample of 44 radio-selected galaxies, five out of 26 in GOODS-N and three out of 18 are detected at 70 μm above 3σ. These eight galaxies make up the sample we discuss in this paper. The positional offsets between the 70 μm centroids and the VLA radio positions are no more than 5 arcsec, which is sufficiently smaller than the 70 μm beam size and astrometric uncertainty. See Table 1 for a summary of the observational data. We use the remaining 21 GOODS-N 70 μm undetected galaxies in a stacking test described in Section 3.6 (the Lockman sample is excluded for this test since its 70 μm map has a much shallower depth).

All sources were observed with the Multi-Element Radio Linked Interferometer Network (MERLIN; Thomasson 1986; Muxlow et al. 2005), yielding high-resolution 0.3 arcsec (GOODS-N) and 0.5 arcsec (Lockman Hole) beam 1.4 GHz radio maps. Three of the eight galaxies were included in the Muxlow et al. (2005) catalogue of Hubble Deep Field (HDF) radio sources (RG J123711,RG J123653, and RG J123645). The 1200 μm flux limits come from the Max-Planck Millimetre Bolometer (MAMBO; Greve et al. 2008) and 850 μm flux limits from Submillimetre Common-User Bolometer Array (SCUBA) (Borys et al. 2003; Coppin et al. 2006). Both fields are covered with *Spitzer* Infrared Array Camera (IRAC) (3.6, 4.5, 5.8, and 8.0 μm) and Multiband Imaging Photometer for Spitzer (MIPS) (24 and 70 μm), however, at greater depths in all bands in GOODS-N. Optical photometry in GOODS-N is from the *Hubble Space Telescope* (*HST*) Advanced Camera for Surveys (ACS[1]) using the F435W, F606W, F814W and F850LP filters (*B, V, i* and z bands). The Lockman Hole has *HST* ACS F814W only (PI: Chapman *HST*

[1] Based on observations made with the NASA/ESA *HST*, and obtained from the Hubble Legacy Archive, which is a collaboration between the Space Telescope Science Institute (STScI/NASA), the Space Telescope European Coordinating Facility (STECF/ESA) and the Canadian Astronomy Data Centre (CADC/NRC/CSA).

7057). One source in Lockman Hole (RG J105146) is not covered by ACS, so we use Subaru/Suprime-Cam *i*-band instead (Miyazaki et al. 2002). The GOODS-N sources have X-ray coverage from the Chandra Deep Field–North (CDF-N). All are formally undetected in the Alexander et al. (2003) catalogue above 5σ in the full band (0.5–8.0 keV), yet four sources are marginally detected at fluxes $<6 \times 10^{-16}$ erg s^{-1} cm^{-2}. Lockman Hole sources have X-ray coverage from *XMM–Newton* (Brunner et al. 2008), and none of the sources are formally detected, with a sensitivity limit in the soft band (0.5–2.0 keV) of 1.9×10^{-16} and 9×10^{-16} erg cm^{-2} s^{-1} in the hard band (2.0–10.0 keV). No X-ray signal is detectable in a stack of the Lockman Hole sources.

3 RESULTS

3.1 Dust temperature

We fit FIR spectral energy distributions (SEDs) to the FIR flux densities (at 70, 850 and 1200 μm) using a modified blackbody emission curve where

$$S_\nu \propto \frac{\nu^{3+\beta}}{\exp(h\nu/kT_\mathrm{d}) - 1}. \quad (1)$$

S_ν is the observed flux density at rest frequency ν, T_d is the characteristic dust temperature and β is the dust's emissivity. Since we are limited by a lack of data points in the FIR, we must assume that the FIR/radio correlation holds (i.e. that L_FIR, evaluated from 8–1000 μm, scales linearly with 1.4 GHz radio luminosity; Condon 1992). While recent works (e.g. Bell 2003; Beswick et al. 2008) indicate that the correlation might deviate at higher redshifts and lower flux densities, its effect on the dust temperature calculation would be systematic. The 0.2 dex scatter found for the local FIR-radio relation suggests an additional uncertainty to our T_d estimates. We note that the additional uncertainties would apply equally to the galaxies in this paper as well as the Chapman et al. (2005) SMGs; foremost, we wish to highlight the temperature difference between the two populations rather than their absolute temperatures.

To calculate temperature, we require an additional constraint to reasonably fit the small number of photometric points with a modified blackbody. We fix $\beta = 1.5$ and adopt a single temperature characterization of the emission, although it is recognized that dust components of a range in temperatures are required to accurately describe well studied nearby galaxies (e.g. Dale et al. 2001). We have tested that our fits are relatively insensitive to β by also using $\beta = 2$, and finding only small (<2 K) differences in the fitted T_d. Fig. 1 shows the best fit modified blackbodies and derived temperatures for our galaxy sample. These blackbody SEDs are combined with radio synchrotron emission ($\alpha = 0.8$) which is fit through the 1.4 GHz flux densities. Best-fitting dust temperatures are listed in Table 1.

3.2 Stellar mass

To estimate the galaxies' stellar masses, we combine the photometric points in the optical (*HST* ACS *B*, *V*, *i* and *z* for GOODS-N and *HST* ACS *i* for Lockman Hole) and the near-IR (*Spitzer*-IRAC 3.6, 4.5, 5.8 and 8.0 μm). For $z = 1$–3, these photometric points cover the rest-frame 1.6 μm wavelength where stellar emission peaks. We use the HYPERZ photometric redshift code (Bolzonella, Miralles & Pelló 2000) to fit this photometry to several stellar population SEDs (Coleman, Wu & Weedman 1980). The optimized stellar population fits are shown in Fig. 2. Measured output includes internal extinction factor A_V and rest-frame *K*-band magnitude (which we use to measure stellar mass with the method outlined by Borys et al. 2005, assuming a mean light-to-mass ratio of $L_\mathrm{K}/M = 3.2$). This analysis indicates that the systems are quite massive and comparable to the stellar masses of the Borys et al. SMGs, with mean $M_\star \sim 2 \times 10^{11}$ M$_\odot$. We note that Alexander et al. (2008) and Chapman et al. (2009) point out that the Borys et al. method of using *K*-band luminosities overestimates stellar masses since it does not correct for the AGN contribution to 8 μm flux density or sample the stellar emission at its peak; while also a probable systematic error in our data set, the effect applies equally to SMGs and hot-dust ULIRGs. Only one source, RG J123711, shows an excess 8 μm flux, indicative of AGN power-law emission; its stellar mass is likely overestimated. Derived stellar masses are listed in Table 1.

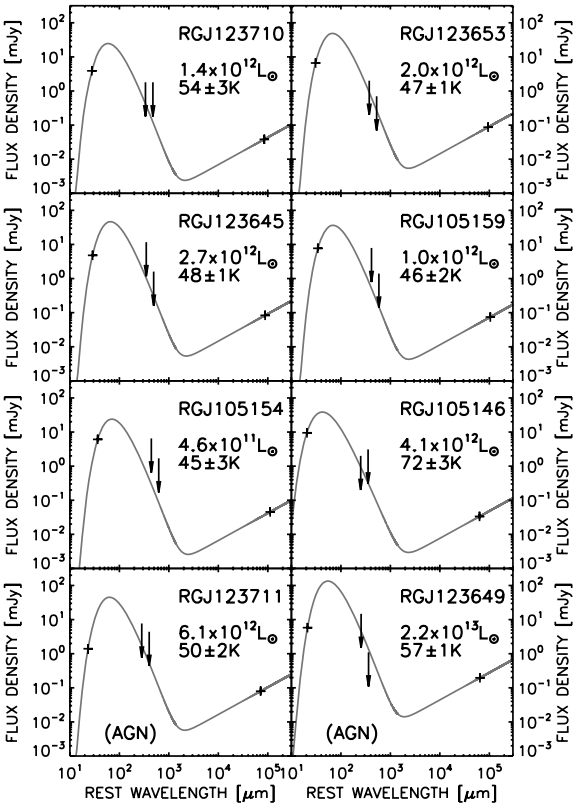

Figure 1. FIR to radio SEDs of eight hot-dust ULIRGs. Each galaxy is fit with a modified blackbody SED to the 70 μm flux density, limits at 850 and 1200 μm, and radio luminosity (which is taken to relate directly to L_FIR via the FIR/radio correlation). On this plot, there is no visible difference between $\beta = 1.5$ and 2 fits. Insets on each panel are the galaxy name, FIR luminosity (integrated from 8–1000 μm) and best-fitting dust temperature. The two panels marked with (AGN) show the SEDs for galaxies who show some evidence of containing luminous AGN (details described in Section 3.4).

3.3 MERLIN radio morphology

We use the high-resolution MERLIN radio maps to assess the contribution of AGN to these galaxies by considering their radio morphology, which is shown as contour overlays on optical imaging in Fig. 3. With resolutions of 0.3 and 0.5 arcsec per beam (for GOODS-N and the Lockman Hole, respectively), the smallest resolvable structure at $z \sim 1.5$ would be 3–5 kpc across; however, the typical size of an AGN emission region at radio wavelengths is much less than 1 kpc. This implies that an AGN dominated source would

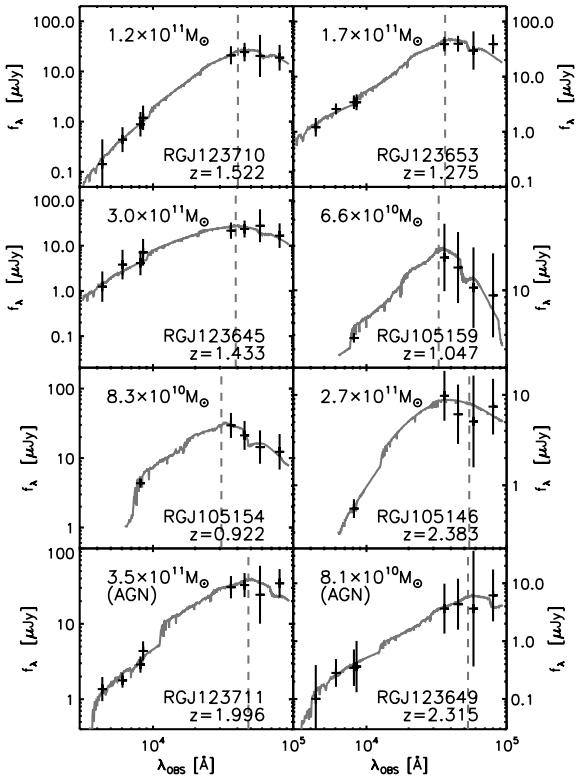

Figure 2. Optical and near-IR photometry points are fit with stellar population models. From these SED fits, we interpolate rest *K*-band magnitudes and compute stellar masses using the method of Borys et al. (2005); the derived stellar masses are given on each panel in the upper left. We also assess the AGN content based on an observed 8 μm flux excess, which is only statistically significant in the spectrum of RG J123711. We mark the redshifted 1.6 μm stellar bump with a dashed vertical line. The two panels marked with (AGN) show the SEDs for galaxies who show some evidence of containing luminous AGN (details described in Section 3.4).

be completely unresolved in MERLIN radio maps (e.g. Casey et al. 2009). Fig. 3 shows that each of these galaxies has extended emission regions on 8 kpc scales, suggestive of spatially distributed star formation, unlikely to be generated by AGN. The effective radii corresponding to the surface areas of the radio emission regions ($>3\sigma$) are given in Table 1. While the morphologies are irregular, we find that the effective radii average to 2.5 ± 0.6 kpc, which agrees with the size measurements of SMGs in (Biggs & Ivison 2008).

3.4 AGN content

As their selection as SFRGs requires, these eight galaxies have rest-frame UV spectral features that are consistent with starbursts and do not exhibit features of active nuclear activity (e.g. no C IV absorption). Except for RG J123649, their X-ray luminosities (we assume $\Gamma = 1.8$) are less than 3×10^{43} erg s^{-1}. These low X-ray luminosities are consistent with star-forming galaxies with little contribution from AGN (e.g. Alexander et al. 2005). With the exception of RG J123649 and RG J123711, the six remaining galaxies also have low 24 μm flux densities ($S_{24} < 250$ μJy). Low 24 μm luminosity is more strongly associated with star formation than AGN emission.

The two hot-dust ULIRGs RG J123711 and RG J123649, which have the highest X-ray luminosities and mid-IR luminosities of

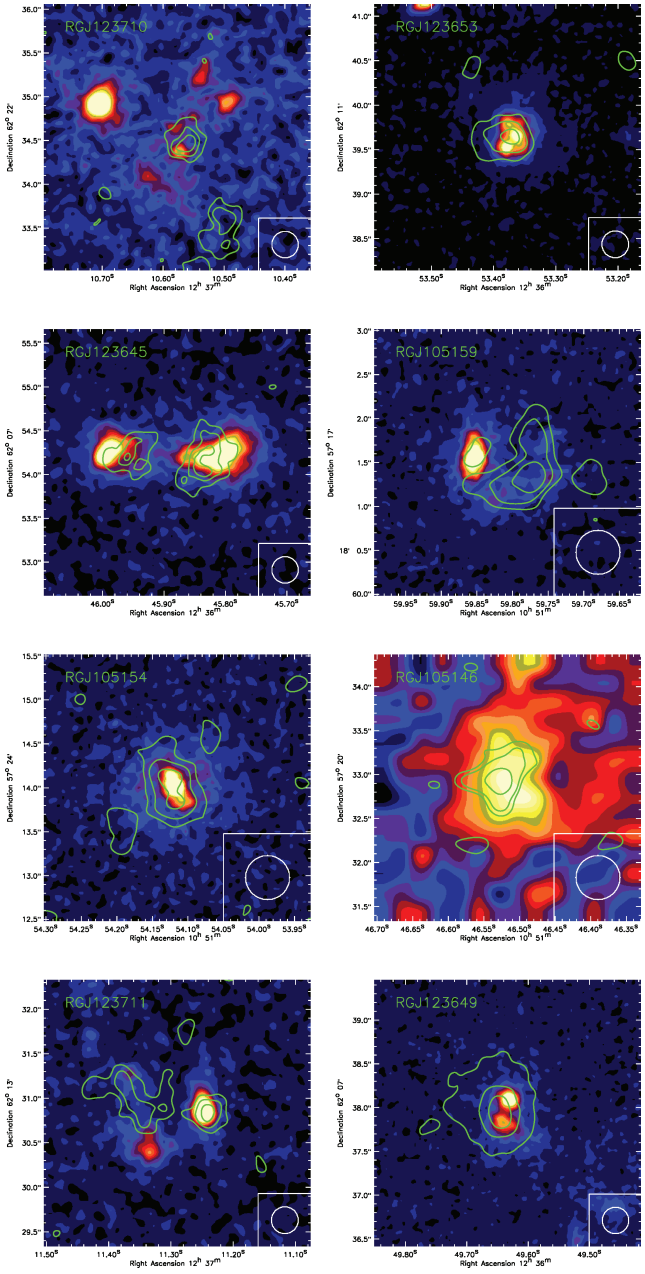

Figure 3. Contours of MERLIN high-resolution 0.3 arcsec radio emission overlaid on *HST* ACS *i*-band imaging for the eight hot-dust ULIRGs. ACS *i*-band imaging was unavailable for RG J105146 and we used Subaru *i*-band in its place. The unresolved MERLIN beam size FWHM is shown in the lower right of each panel in white. The contour levels plotted are 40, 60 and 80 per cent of the peak flux density in each image. Structure in radio emission is seen in each galaxy on 8 kpc scales.

the sample, might contain powerful AGN despite a lack of rest-UV AGN spectral features. The MERLIN radio emission in RG J123711 (bottom left-hand panel in Fig. 3) is separated in two components: an extended region to the NE (63 per cent of the integrated flux), and a bright compact region to the SW (37 per cent). The X-ray source coincides with this SW component. In contrast, a large 10^{10} M$_\odot$ molecular gas reservoir (a strong case that substantial star formation may be present) has been detected in CO and is morphologically separated evenly across the two NE and SW components (Chapman et al. 2008; Casey et al., in preparation). For these reasons, we

believe the NE region is likely a star-forming ULIRG merging with the SW region, an AGN-dominated galaxy.

While the existence of an AGN in RG J123649 is supported by a bright X-ray luminosity and a compact core in optical imaging, there is no sign of AGN activity in the optical spectrum or in its ∼8 kpc extended radio morphology. We estimate that AGN emission is 40 ± 30 per cent and the star-forming component is 60 ± 30 per cent of the radio flux by deconvolving an unresolved 0.3 arcsec Paint Spread Function (PSF) from its radio morphology. We adjust the radio luminosity and inferred star-formation rates (SFRs) of both RG J123711 and RG J123649 to solely represent the estimated star-forming components (see Table 1, 'RG J . . . SF component:'). We have also labelled both galaxies as AGN in Figs 1 and 2 to clarify that they differ from the other six.

It is possible that these two galaxies' 70 μm flux densities are dominated by emission from torus dust surrounding the AGN (which can have very hot-dust temperatures, $T_{\rm D} \sim 1000$ K). However, disentangling the relative contributions of AGN and star formation to 70 μm flux density is beyond the scope of this study since it requires detailed knowledge of the FIR SEDs. For this reason, we exclude RG J123711 and RG J123649 from further analysis of the hot-dust ULIRG aggregate properties, since we wish to characterize the properties of star formation dominated ULIRGs exclusively.

There is no evidence to suggest that the remaining six galaxies contain significantly luminous AGN. With a sample size of eight galaxies, two of which likely contain AGN, the total AGN fraction in the population is 25 per cent. This is consistent with the estimated AGN fraction of SMGs, between 20 and 40 per cent, from Alexander et al. (2005).

3.5 Star formation rates

We estimate SFRs from the VLA radio luminosities, using the radio/FIR correlation for star-forming galaxies (Condon 1992; Helou, Soifer & Rowan-Robinson 1985; Sanders & Mirabel 1996). We abstain from calculating UV-inferred SFRs since they would be subject to significant (yet uncertain) extinction factors (as evidenced by the irregular MERLIN radio morphologies relative to the distribution of rest-UV flux in Fig. 3). The FIR luminosities derived from the radio are consistent with the submm detection limits and the flux densities at 70 μm as shown in Fig. 1. The inner quartile (25–75 per cent) of SFRs in this sample is 200–1100 $\rm M_\odot\ yr^{-1}$ (both derived quantities, $L_{\rm FIR}$ and SFR are given in Table 1).

SFR densities are found by dividing these SFRs by the surface areas of MERLIN radio emission regions. Comparing these SFR densities to their theoretical maximum – the maximum gas density divided by the local dynamical time (see equation 5 of Elmegreen 1999 we use $t_{\rm dyn} = 4 \times 10^7$ yr) – we can determine if the implied SFR density exceeds the theoretical prediction. While local ULIRGs with $\Sigma_{\rm SFR} \approx 200\,\rm M_\odot\ yr^{-1}\ kpc^{-2}$ are forming stars at their theoretical maximum (e.g. Tacconi et al. 2006), none of the galaxies come within a factor of four of exceeding their maximum SFR density limits.

We note that one of the eight galaxies of our sample, RG J123710, has been detected in CO gas by Daddi et al. (2008). The presence of a molecular gas reservoir $>10^{10}\,\rm M_\odot$ indicates that high levels of star formation ($>100\,\rm M_\odot\ yr^{-1}$) can potentially occur. In their interpretation of the detection, Daddi et al. claims that RG J123710 is most likely a spiral galaxy undergoing modest-efficiency star formation lower than most SMG ULIRGs. However, our detection of RG J123710 at 70 μm directly confirms that it is a ULIRG. More CO observations are needed to investigate if the rest of the hot-dust ULIRG population exhibits modest star formation efficiencies or high, SMG-like efficiencies (Casey et al., in preparation).

3.6 70 μm undetected SFRGs

Our eight galaxy sample likely represents the most luminous subsample of the hot-dust ULIRG population because of the current limitations in 70 μm surveys. To investigate the possible lower luminosity extension of the population, we analyse the 21 GOODS-N galaxies which were selected as SFRGs but not detected at 70 μm (the Lockman sample is excluded since its 70 μm coverage has a much shallower depth). Here, we stack 70 μm cutouts of these 21 SFRGs, centred on their VLA positions. We use the stacking method described in Huynh et al. (2007) and Hainline et al. (in preparation) which was used to stack ∼68 70 μm undetected SMGs. We have a detection of 0.45 ± 0.15 mJy in the SFRG stacked image at 3.0σ, which is comparable to the 0.48 ± 0.15 mJy 3.2σ detection for the SMGs of Hainline et al. (in preparation). This indicates that SMGs and 70 μm undetected SFRGs likely have similar 70 μm luminosities, although larger samples of SFRGs are needed to see if their relative detection rates at 70 μm are similar. Because of their detection at 70 μm, the eight SFRGs of this paper are likely the highest luminosity ($z < 3$) and potentially the hottest dust temperature specimens of the SFRG population.

4 DISCUSSION

4.1 Volume density

The volume density is estimated by constraining the density of galaxies satisfying our selection criteria. The density of these 70 μm detected ULIRGs is $1.4 \times 10^{-5}\,\rm Mpc^{-3}$. However, the difference in volume density estimates between GOODS-N and Lockman Hole, which is expected due to the 70 μm sensitivity differences between the two fields, prevents us from constraining the hot-dust ULIRG luminosity function well.

While this explicit population of hot-dust ULIRGs is ∼5× more rare than SMGs, there likely exists a larger population of $z > 1$ ULIRGs with hot-dust temperatures. First, spectroscopic incompleteness of ∼50 per cent suggests the sample is likely twice as large (although it is noted that SMGs are also affected by spectroscopic incompleteness). Secondly, there are likely additional ULIRGs at $z \sim 2$ undetected in the radio (for instance, from scatter in the FIR/radio relation). Finally, the 70 μm sensitivity limits of these maps do not exclude many of the other SFRGs in our parent sample from having warm enough dust to still represent hotter ULIRGs than SMGs. As we have shown in our analysis of the GOODS-N sample, proportionally more SFRGs are 70 μm detected than SMGs; as also indicated by the stacked result of 70 μm undetected SFRGs, many more SFRGs might become 70 μm detected if the GOODS-N 70 μm depth can be achieved in other fields. The *Herschel Space Observatory* will dramatically improve the uniformity and depth of 70 μm coverage (confusion limit of 0.04 mJy at 2σ), potentially discovering many of the ULIRGs that lay just below the current MIPS detection limits.

4.2 Selection effect in $L_{\rm FIR} - T_{\rm d}$ and redshift

Fig. 4 illustrates the selection effects of IR-wavelength observations as a function of FIR luminosity and characteristic dust temperature. Assuming the radio/FIR correlation, radio detection is independent of dust temperature. At $z = 2$, a $10^{13}\,\rm L_\odot$ system is only detectable

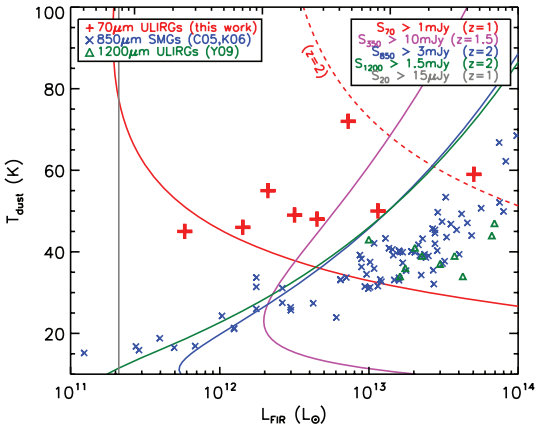

Figure 4. FIR luminosity against dust temperature illustrates the temperature/luminosity biases of different single-wavelength detection techniques, at 70 μm (red), 350 μm (magenta), 850 μm (blue), 1200 μm (green) and 20 cm/1.4 GHz radio (grey). The boundaries on the plot are determined by flux density 2σ upper limits for these observations: 1 mJy at 70 μm, 10 mJy at 350 μm, 3 mJy at 850 μm, 1.5 mJy at 1200 μm and 10 μJy at 20 cm (the limits for GOODS-N). The boundaries also represent a limit in redshift which is chosen based on the characteristic mean redshift of sources detected at that wavelength. Sources may be detected at the given wavelength on the high-luminosity side of each boundary. We overplot the SMG population which is selected at 850 μm (Chapman et al. 2005; Kovács et al. 2006), and z ∼ 2 1200 μm luminous ULIRGs from the EGS field (Younger et al. 2009), and the sample in this paper, detected at 70 μm with a $z = 1$ boundary (solid) and $z = 2$ boundary (dashed).

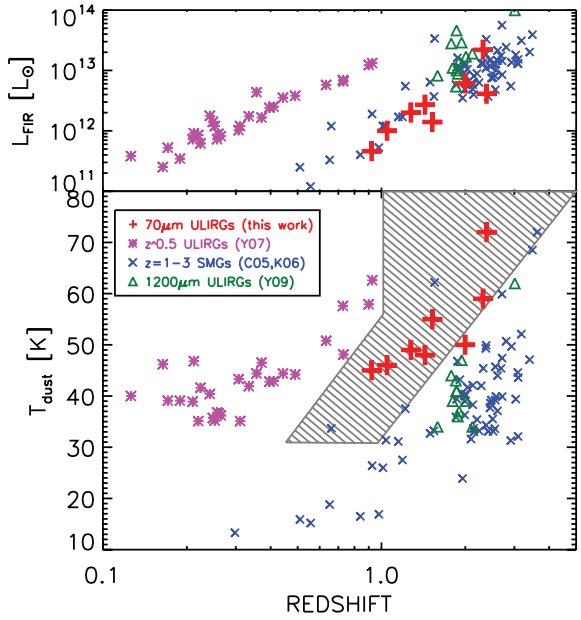

Figure 5. FIR luminosity and dust temperature as functions of redshift (log scale), with the same symbols as in Fig. 4, with a low redshift 350 μm galaxy population overplotted for comparison (Yang et al. 2007). Above, the 70 μm has similar luminosities to SMGs at the same redshifts. Below we highlight the poorly explored region (shaded region) in dust temperature with redshift. The 70 μm selected sample begins to sample this unexplored area.

at 850 μm or 1200 μm if it has $T_d < 40$ K. Since the mean redshift of radio-detected SMGs is $z = 2.2$, the dust temperature selection effect significantly impacts the proposed surface density of ULIRGs and thus their contribution to the global SFR density near $z \sim 2$. If instead we select objects by the methods of this paper at 70 μm, the dust temperature selection effect is inverted, and detection is possible for the hottest $z \sim 2$ sources ($T_d > 70\,K$). By lowering the redshift boundary from $z > 2$ to $z > 1$, detection is possible for 10^{13} L$_\odot$ galaxies that have $T_d > 35$ K.

While the FIR selection functions have hard boundaries in L_{FIR} and T_d, their dependence on redshift is important. From Fig. 4, we see that 70 μm selection is not ideal for $z > 2$ samples where it is limited to temperatures $T_d \gtrsim 70$ K, whereas at $z \sim 1$ it can select a wider range of ULIRGs with $T_d \gtrsim 40$ K. In Fig. 5, we show the projections of both L_{FIR} and T_d with redshift. This highlights that the luminosities of the 70 μm-selected sample are comparable to SMGs at the same redshift. However, as a function of dust temperature, the 70 μm galaxies occupy an unexplored region in $z - T_d$ which is heavily restricted by the selection biases illustrated in Fig. 4.

4.3 Comparison of SED shape to SMGs

A direct comparison of the observationally derived SED for these hot-dust ULIRGs with SMGs is shown in Fig. 6. We average the 70 μm detections, 850 μm upper limits, and radio detections of the six star formation dominant hot-dust ULIRGs to form our composite SED; the composite SED adopts the mean redshift ($z = 1.5$), FIR luminosity (1.9×10^{12} L$_\odot$) and dust temperature (52 K) of the six galaxy sample. Since SMGs have a mean redshift of 2.2, we take several comparable subsamples of GOODS-N and Lockman Hole SMGs to generate an average SMG SED with mean redshift 1.5. The resulting mean luminosity of this SMG subsample is 2.2×10^{12} L$_\odot$ with dust temperature 36 K.

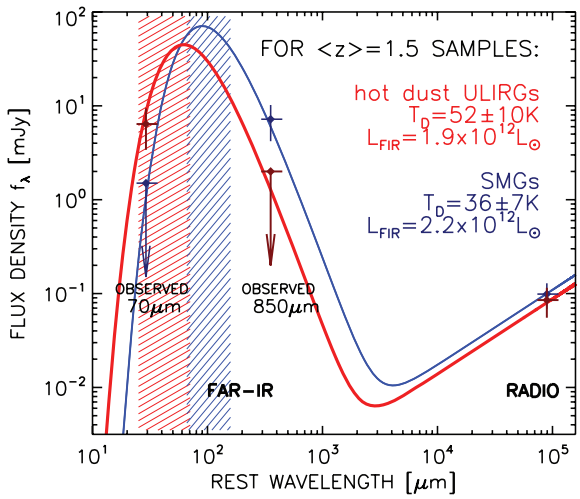

Figure 6. A composite spectrum of the six star-forming, 70 μm detected, hot-dust ULIRGs relative to a composite SED for a subsample of SMGs with $\langle z \rangle = 1.5$. We select several subsamples of SMGs all with mean redshift 1.5 to mimic the redshift distribution of the hot-dust ULIRGs. The average flux densities for hot-dust ULIRGs are 6.4 mJy at 70 μm, <2 mJy at 850 μm and 50 μJy at 20 cm. The flux density points for SMGs are <1.5 mJy at 70 μm, 7 mJy at 850 μm and 60 μJy at 20 cm. The red and blue vertical bands illustrate the range of peak fluxes corresponding to two temperature regimes; blue represents 36 ± 7K and submm detected, while red represents 52 ± 10K. Note that at 350 μm, both samples of 70 and 850 μm galaxies would be equally easy to detect.

Based on these SED fits, we do not expect SMGs to be detected at 70 μm. This agrees with observations; nearly all SMGs (68/73, >93 per cent) are undetected <3σ at 70 μm (Hainline et al. in preparation). Those that are 70 μm-detected are at low-z and have

higher luminosities than most SMGs at low redshifts. To compare the SMG and SFRG populations, we compare their 70 μm detection rates. We limit this test to $z < 2$ since the redshift selection functions for the populations differ (submm + radio selection and radio selection have different redshift biases; see Chapman et al. 2005). This removes most effects of redshift bias from radio detection in both samples. SMGs and SFRGs have similar radio luminosities, so the same fraction of each should be detected at 70 μm if they have the same distributions in dust temperature. In GOODS-N, where the observations are deepest and the most complete, 4/8 (50 ± 25 per cent) z < 2 submm-faint radio galaxies are detected at 70 μm but only 1/14 (7 ± 7 per cent) of submm-bright radio galaxies (SMGs) are detected (Chapman et al. 2005; Pope et al. 2006, 2008). The Lockman Hole observations do not have nearly the depth as those of GOODS-N and thus have fewer sources; however, the statistics are consistent with the finding in GOODS-N, with 3/7 (43 ± 25 per cent) submm-faint galaxies detected at 70 μm and only 1/5 (20 ± 20 per cent) SMGs detected. Therefore, in contrast to SMGs, galaxies selected by our method (SFRG selection) are far more likely to be detected at 70 μm (30-50 per cent).

4.4 Comparison to other IR selection techniques

Since the advent of *Spitzer* and other IR observatories, the population of dusty galaxies studied at high redshift has grown substantially. Many of these galaxies are more bolometrically luminous than typical UV-selected galaxies, but they may be poorly understood as a population due to faintness in the optical. Furthermore, the optical counterparts for 850 and 70 μm sources are not easily identified due to the ∼12–20 arcsec beam size; for these reasons, substantial portions of SMGs and ULIRGs have no redshift identification. Similar problems exist for other IR-selected galaxies. Here, we contrast the hot-dust ULIRGs in this paper to other IR-selected, dusty galaxy populations at $z \sim 2$, noting potential overlap of selection techniques.

To circumvent the problems that arise from FIR selection (increased beam size and poor sensitivity limits), many dusty galaxies are selected in the mid-IR by their observed 24 μm flux densities. However, the selection of dusty star-forming LIRGs and ULIRGs through mid-IR 24 μm continuum diagnostics is frequently contaminated by power-law emission from AGN, and inferring star formation properties can require large correction factors to bolometric luminosity (e.g. Dale et al. 2005; Papovich et al. 2005). All eight galaxies in our sample are classified as Dust Obscured Galaxies (DOGs; Dey et al. 2008; Pope et al. 2008); however, the selection criteria of DOGs is so broad that without detailed additional information (the radio maps, FIR detections and non-detections and near-IR photometry), it is difficult to understand the importance or evolutionary significance of this classification. We further emphasize that 3/8 specimens in our 70 μm sample have $S_{24} < 300$ μJy (and are only selected as DOGs under the selection described by Pope et al.), revealing that ultraluminous activity at $z = 1$–3 can be missed by 24 μm selection criteria.

A recent study by Younger et al. (2009) presents 12 $z \sim 2$ ULIRGs in the Extended Groth Strip (EGS) field, selected in the *Spitzer* IRAC and MIPS bands and followed up with MAMBO at 1200 μm (where 9/12 are detected). They have a characteristic dust temperature 41 ± 5 K (using $\beta = 1.5$ modified blackbody fits) and are shown in Figs 4 and 5. The 12 Younger et al. galaxies bridge the gap between SMGs and hot 70 μm detected sources in temperature but are much more luminous than the 70 μm sample. They have a mean 1200 μm flux density of ∼1.6 mJy where our 70 μm sample is uniformly undetected.[2] This would imply that the 12 EGS galaxies have 850 μm flux densities ∼3–6 mJy, FIR luminosities (8–1000 μm) $>10^{13}$ $L_\odot$ and thus could be classified as SMGs. The selection of the Younger et al. sample in the mid-IR, by the presence of a prominent stellar bump in IRAC photometry and dust at 24 μm, is similar to the DOG selection, although with a few additional constraints reveals a potentially strong probe of ultraluminous activity at high redshift. However, more far-IR observations of $z \sim 2$ mid-IR selected samples are needed to assess the selection's completeness in choosing both star-forming ULIRGs and AGN dominated ULIRGs at $z > 1$.

Selection at 350 μm at $z \sim 2$ has similar temperature biases as 850 and 1200 μm due to its high flux limit ($S_{350} > 10$ mJy at 2σ). As seen in Fig. 6, 350 μm selection at $z \sim 1.5$ has the potential to select SMGs and hot-dust ULIRGs equally well since it samples the dust SED near its peak for a wide range of temperatures. However, until the depth of 350 μm imaging can be improved, current observing facilities allow only 350 μm detections of the most luminous or low redshift sources (e.g. Yang et al. 2007). The Balloon-borne Large Aperture Submillimeter Telescope (BLAST) has recently mapped the Chandra Deep Field South at 250, 350 and 500 μm at greater depth than has been done before in any field at those wavelengths (Devlin et al. 2009). While useful for measuring the flux densities of already known ULIRGs and high-redshift galaxies, only ∼12 $z > 1$ galaxies are detected and found to have robust counterparts (Dye et al. 2009). When it begins full operations, the *Herschel Space Observatory* will be another observing tool at 350 μm and will dramatically improve the depth of 70 μm observations in many heavily observed fields, thus providing better statistics at shorter FIR wavelengths. In addition, future work from the SCUBA2 instrument at 450 μm have the potential to expand the sample of $z \sim 1$–3 ULIRGs through deeper observations near the peak of the dusts' SED.

5 CONCLUSIONS

This paper has observationally demonstrated that submillimetre wavelength observations of galaxies at $z \sim 1$–3 have a strong temperature bias which preferentially detects galaxies with cooler dust temperatures. By selecting ULIRGs that are detected at 70 μm (and verifying that they are starburst dominated), we have found a set of galaxies which are undetected in the submillimetre yet still represent some of the most luminous systems at $z > 1$. Their volume density is 1.4×10^{-5} Mpc^{-3}, approximately 5× more rare than SMGs, although this has likely been underestimated due to spectroscopic incompleteness and large variations in the sensitivity limits of 70 μm surveys.

Like most IR-selected dusty galaxies, the SFRs in these hot-dust ULIRGs are on average much higher than the majority of UV-selected star-forming galaxies at the same epoch. While some UV-selected sources have high stellar masses (Shapley et al. 2005, Hainline et al., in preparation), they show consistently lower SFRs, reiterating that the UV misses the most dramatic star-forming galaxies at high redshift. Due to their similarity with SMGs (in terms of stellar mass, UV-spectra, FIR and radio luminosities), the hot-dust ULIRGs represent an extension of SMGs towards a wider range of dust temperatures at $z \sim 1$–3, similar to the already observed wide range in dust temperatures seen in local ULIRGs.

[2] The depth of MAMBO coverage in GOODS-N is ∼0.7–0.8 mJy rms compared to the ∼0.4 mJy photometric rms of the EGS pointings, while Lockman Hole has 0.8–1.0 mJy rms.

We have shown that AGN contribute little to the FIR luminosities in six of the eight hot-dust ULIRGs. The detection of extended radio emission (with typical radii 2–3 kpc) suggests spatially distributed star formation rather than compact AGN. In addition, the UV-spectral properties and low X-ray luminosities are consistent with star formation. The two ULIRGs that do show signs of AGN activity also have evidence for substantial star formation and are, therefore, comparable to SMGs which contain bright AGN.

Combining our hot-dust ULIRG population with the SMGs results in a sample of $z \sim 2$ ULIRGs with less temperature-dependent bias than the SMG population alone. However, we have shown that searches for high redshift FIR luminous galaxies are likely still somewhat incomplete. Even at $z \sim 2$, there are likely other FIR luminous galaxies which are not well characterized by current submm or FIR observations. *Herschel Space Observatory* and SCUBA2 will help push detection of more $z > 1$ ULIRGs in the 50–500 μm range while more work with deeper radio observations (from *e*-MERLIN and EVLA) will be needed to find potential ULIRG activity beyond $z > 3$. By working towards completeness in the $z > 1$ ULIRG population, we will learn about the role of heavy, short-lived star formation in the formation and evolution of galaxies in the early Universe.

ACKNOWLEDGMENTS

We thank the anonymous referee for helpful comments which improved the paper. This work is based, in part, on observations made with MERLIN, a National Facility operated by the University of Manchester at Jodrell Bank Observatory on behalf of STFC, and the VLA of the National Radio Astronomy Observatory, a facility of the National Science Foundation operated under cooperative agreement by Associated Universities, Inc. CMC thanks the Gates-Cambridge Trust, and IRS thanks STFC for support.

REFERENCES

Alexander D. M. et al., 2003, AJ, 126, 539
Alexander D. M., Bauer F. E., Chapman S. C., Smail I., Blain A. W., Brandt W. N., Ivison R. J., 2005, ApJ, 632, 736
Alexander D. M. et al., 2008, AJ, 135, 1968
Bell E. F., 2003, ApJ, 586, 794
Beswick R. J., Muxlow T. W. B., Thrall H., Richards A. M. S., Garrington S. T., 2008, MNRAS, 385, 1143
Biggs A. D., Ivison R. J., 2006, MNRAS, 371, 963
Biggs A. D., Ivison R. J., 2008, MNRAS, 385, 893
Blain A. W., 1999, MNRAS, 304, 669
Blain A. W., Smail I., Ivison R. J., Kneib J.-P., Frayer D. T., 2002, Phys. Rep., 369, 111
Blain A. W., Chapman S. C., Smail I., Ivison R., 2004, ApJ, 611, 52
Bolzonella M., Miralles J.-M., Pelló R., 2000, A&A, 363, 476
Borys C., Chapman S., Halpern M., Scott D., 2003, MNRAS, 344, 385
Borys C., Smail I., Chapman S. C., Blain A. W., Alexander D. M., Ivison R. J., 2005, ApJ, 635, 853
Brunner H., Cappelluti N., Hasinger G., Barcons X., Fabian A. C., Mainieri V., Szokoly G., 2008, A&A, 479, 283
Casey C. M., Chapman S. C., Muxlow T. W. B., Beswick R. J., Alexander D. M., Conselice C. J., 2009, MNRAS, 395, 1249
Chapman S. C., Smail I., Blain A. W., Ivison R. J., 2004, ApJ, 614, 671
Chapman S. C., Blain A. W., Smail I., Ivison R. J., 2005, ApJ, 622, 772
Chapman S. C. et al., 2008, ApJ, 689, 889
Chapman S. C., Blain A. W., Ibata R., Ivison R. J., Smail I., Morrison G., 2009, ApJ, 691, 560
Coleman G. D., Wu C.-C., Weedman D. W., 1980, ApJS, 43, 393
Condon J. J., 1992, ARA&A, 30, 575
Coppin K. et al., 2006, MNRAS, 372, 1621
Daddi E., Dannerbauer H., Elbaz D., Dickinson M., Morrison G., Stern D., Ravindranath S., 2008, ApJ, 673, L21
Dale D. A., Helou G., Contursi A., Silbermann N. A., Kolhatkar S., 2001, ApJ, 549, 215
Dale D. A. et al., 2005, ApJ, 633, 857
Devlin M. et al., 2009, Nature, 458, 737
Dey A. et al., 2008, ApJ, 677, 943
Dye S. et al., 2009, ApJ, submitted (arXiv:0904.1206)
Eales S., Lilly S., Webb T., Dunne L., Gear W., Clements D., Yun M., 2000, AJ, 120, 2244
Elmegreen B. G., 1999, ApJ, 517, 103
Greve T. R., Pope A., Scott D., Ivison R. J., Borys C., Conselice C. J., Bertoldi F., 2008, MNRAS, 389, 1489
Helou G., Soifer B. T., Rowan-Robinson M., 1985, ApJ, 298, L7
Hinshaw G. et al., 2009, ApJS, 180, 225
Huynh M. T., Pope A., Frayer D. T., Scott D., 2007, ApJ, 659, 305
Kovács A., Chapman S. C., Dowell C. D., Blain A. W., Ivison R. J., Smail I., Phillips T. G., 2006, ApJ, 650, 592
Levine D. A. et al., 1998, ApJ, 504, 64
Miyazaki S. et al., 2002, PASJ, 54, 833
Muxlow T. W. B. et al., 2005, MNRAS, 358, 1159
Papovich C., Dickinson M., Giavalisco M., Conselice C. J., Ferguson H. C., 2005, ApJ, 631, 101
Pope A. et al., 2006, MNRAS, 370, 1185
Pope A. et al., 2008, ApJ, 689, 127
Reddy N. A., Steidel C. C., Erb D. K., Shapley A. E., Pettini M., 2006, ApJ, 653, 1004
Rieke G. H., Alonso-Herrero A., Weiner B. J., Perez-Gonzalez P. G., Blaylock M., Donley J. L., Marcillac D., 2009, ApJ, 692, 556
Sanders D. B., Mirabel I. F., 1996, ARA&A, 34, 749
Shapley A. E., Steidel C. C., Erb D. K., Reddy N. A., Adelberger K. L., Pettini M., Barmby P., Huang J., 2005, ApJ, 626, 698
Smail I., Ivison R. J., Blain A. W., Kneib J.-P., 2002, MNRAS, 331, 495
Tacconi L. J. et al., 2006, ApJ, 640, 228
Thomasson P., 1986, QJRAS, 27, 413
Yang M., Greve T. R., Dowell C. D., Borys C., 2007, ApJ, 660, 1198
Younger J. D. et al., 2009, MNRAS, 394, 1685

This paper has been typeset from a TEX/LATEX file prepared by the author.